High Spatial Resolution and high sensitivity X-ray Fluorescence Imaging

Lei Xing , Ph.D., Jacob Haimson Professor

Department of Radiation Oncology

Molecular Imaging Program at Stanford (MIPS)

Department of Electrical Engineering

Stanford University School of Medicine

7/14/2015

Available Imaging Tools

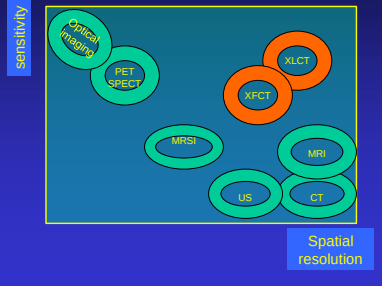

@01-258_via99-011_hepatoma_onscreen

X-ray Fluorescence Molecular CT Imaging

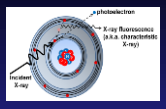

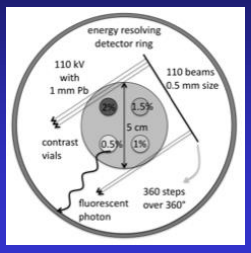

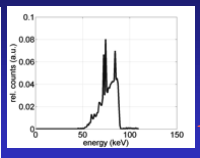

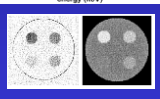

M. Balazova, Y. Kuang, G. Pratx, L. Xing, X-ray Fluorescence Molecular CT Imaging, IEEE Trans Med Ima., 2012

X-ray Fluorescence Molecular CT Imaging

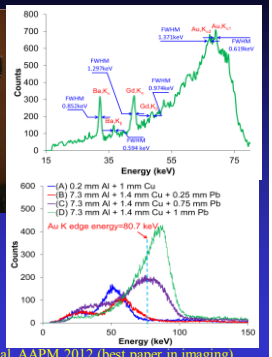

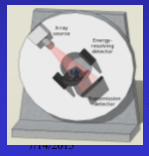

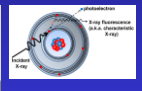

Fig. 1. (left) Proposed XFCT-CT system. (top) Physical mechanism of X-ray fluorescence from K-shell electrons.

K. Yu et al, AAPM 2012 (best paper in imaging)
Medical Physics Letters, 2013.

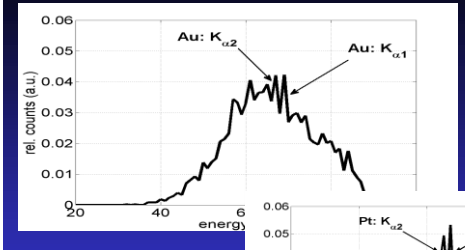

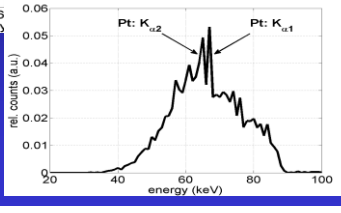

@01-258_via99-011_hepatoma_onscreen

Sensitivity

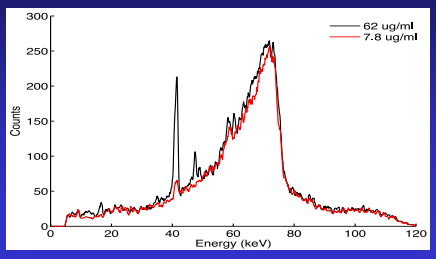

X-ray Fluorescence/Luminescence Tomography

G. Pratx et al. IEEE Trans. Med. Ima., 2010

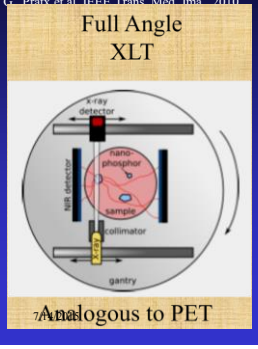

Reconstruction: ML-EM

Noise from counting statistics: $Y_i \sim \text{Poisson}(y_i)$

Log-likelihood: $\log p_{\mathbf{m}}(\mathbf{y}) = \sum_{i=1}^{P} -y_i + m_i \log(y_i) - \log(m_i!)$

$$\begin{aligned} \text{maximize} \quad & f_{\mathbf{m}}(\mathbf{y}) = \sum_{i=1}^{P} -y_i + m_i \log(y_i) \\ \text{subject to} \quad & \mathbf{y} = A\mathbf{x} \\ & \mathbf{x} \geq 0 \end{aligned}$$

Expectation-Maximization: $x_j^{n+1} = \frac{x_j^n}{N_j} \sum_{i=1}^{P} a_{ij} \frac{m_i}{\sum_{b=1}^{N} a_{ib} x_b^n + \hat{n}_D}$

@01-258_via99-011_hepatoma_onscreen

X-ray Fluorescence Molecular CT Imaging

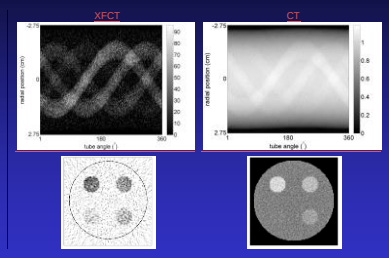

Sinograms (top) and reconstructed CT images (bottom) for XFCT (left) and transmission CT (right) of the low-resolution phantom loaded with gold for a 0.1 mGy imaging dose. (Magda Bozalova et al)

M. Balazova, Y. Kuang, G. Pratx, L. Xing, X-ray Fluorescence Molecular CT Imaging, IEEE Trans Med Ima., 2012

X-ray Fluorescence Molecular CT Imaging

M. Balazova, Y. Kuang, G. Pratx, L. Xing, X-ray Fluorescence Molecular CT Imaging, IEEE Trans Med Ima., 2012

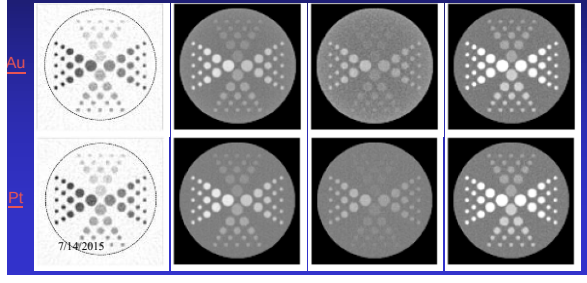

Multiplexing

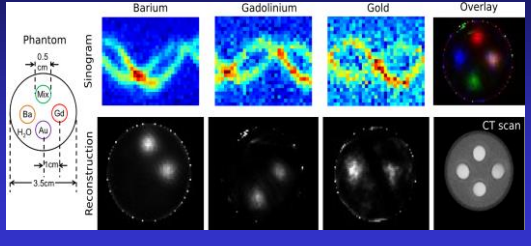

K. Yu et al, AAPM 2012 (best paper in imaging)
Medical Physics Letters, 2013.

@01-258_via99-011_hepatoma_onscreen

Multiplexing

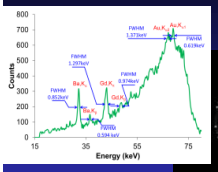

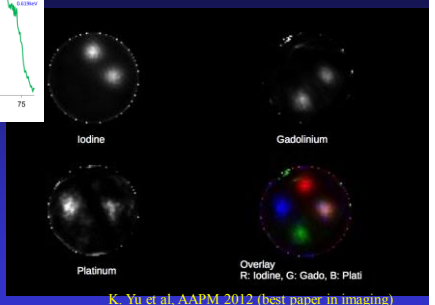

K. Yu et al, AAPM 2012 (best paper in imaging)
Medical Physics Letters, 2013.

Overcoming Compton Scatter

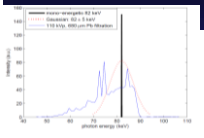

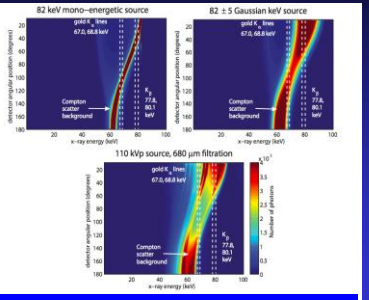

Moiz Ahmad et al, Order of Magnitude Sensitivity Increase in X-ray Fluorescence CT (XFCT) Imaging With an Optimized Spectro-spatial Detector Configuration, IEEE Med Ima, 2013

XFCT Detection Limit

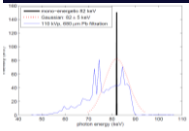

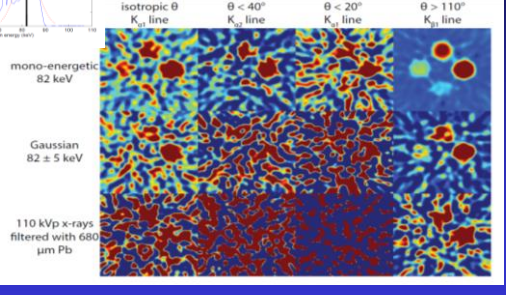

@01-258_via99-011_hepatoma_onscreen

Sensitivity vs Radiation Dose

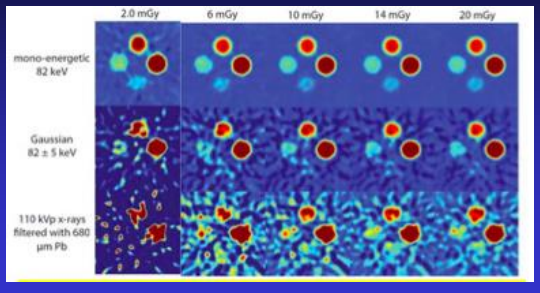

Proton Fluorescence (In collaboration with Hokkaido Unv.)

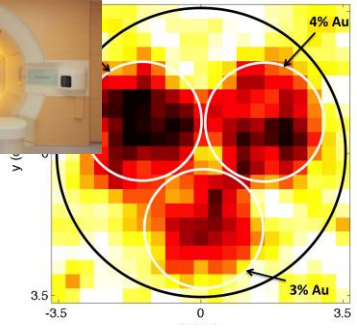

M. Bazalovo et al, Med Phys Lett, 2015,

Going Beyond K-Schell Imaging

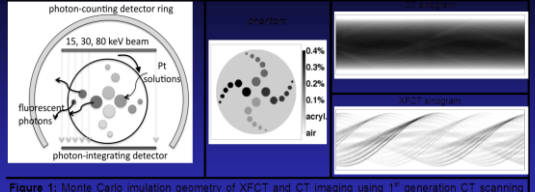

Figure 1: Monte Carlo imulation geometry of XFCT and CT imaging using 1st generation CT scanning (left). Monoenergetic pencil beams with 15, 30, and 80 keV were simulated using 55 dwell positions across the extent of the phantom and rotated by 360 in 1 steps. The 2-cm diameter phantom (middle) contained 0.6 to 2.2 mm diameter vials with 0.1 to 0.4% solutions of Cisplatin. Transmission CT (top right) and XFCT (bottom right) sinograms of the phantom were generated. CT and XFCT images were then reconstructed with three different reconstruction techniques.

Magda Bazalova et al, PMB, 2013

@01-258_via99-011_hepatoma_onscreen

High-sensitivity x-ray fluorescence CT imaging of Cisplatin with L-shell x-rays

Magda Bazalova et al, to be published

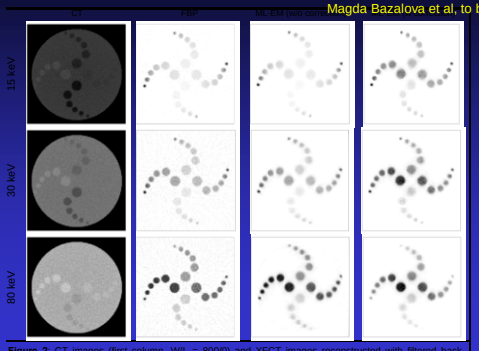

Figure 2: CT images (first column, W/L = 800/0) and XFCT images reconstructed with filtered back-projection (FBP, second column) and maximum likelihood expectation maximization (ML-EM, 20

High-sensitivity x-ray fluorescence CT imaging of Cisplatin with L-shell x-rays

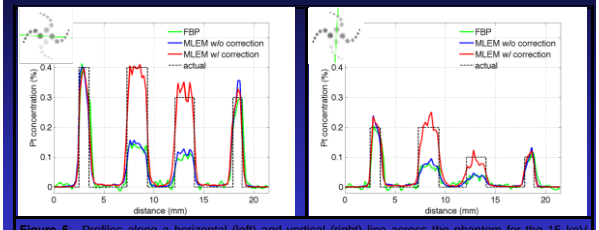

Figure 5: Profiles along a horizontal (left) and vertical (right) line across the phantom for the 15 keV images reconstructed with FBP (green), ML-EM without (blue) and with (red) attenuation correction.The actual profile is marked by the black dashed line. The accuracy of concentration reconstruction is significantly increased when attenuation correction is applied.

Radioluminescence & X-ray Luminescence CT

Principle

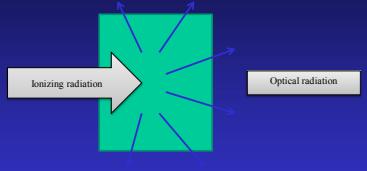

Current applications

- PET and SPECT scintillators
- CT detectors
- Portal imaging
- Dosimetry
- Scintillation counting
- High-energy physics

G. Pratx, 2012

@01-258_via99-011_hepatoma_onscreen

CT Molecular Imaging using nanophosphors

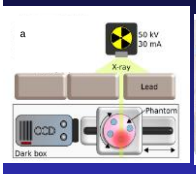

Template

White Light

Pratx, Sun, Carpenter & Xing, Optics Letters, 2011.

QD710-RGD peptide

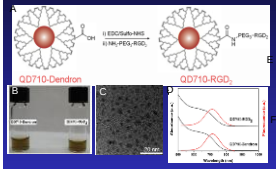

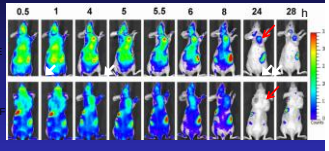

Modification of QD710-Dendron with a dimeric RGD peptide, RGD_2. B: Excellent solubility and monodisperity in aqueous solution for the QD710-Dendron (left) and QD710-RGD_2 (right). C: TEM image of QD710-RGD_2. D: UV absorbance and NIRF of the QD710-Dendron (bottom) and QD710-RGD_2 (top). In vivo NIRF imaging of QD710-RGD_2 (active targeting, E) and QD710-Dendron (passive targeting, F) in mice bearing SKOV3 tumor (Cheng's lab).

Photon yield vs dose

Gd_2O_2S:Eu

LaO_2:Eu

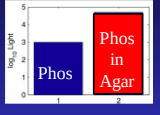

Varian 100keV fluoro

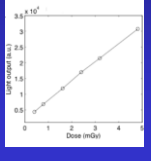

@01-258_via99-011_hepatoma_onscreen

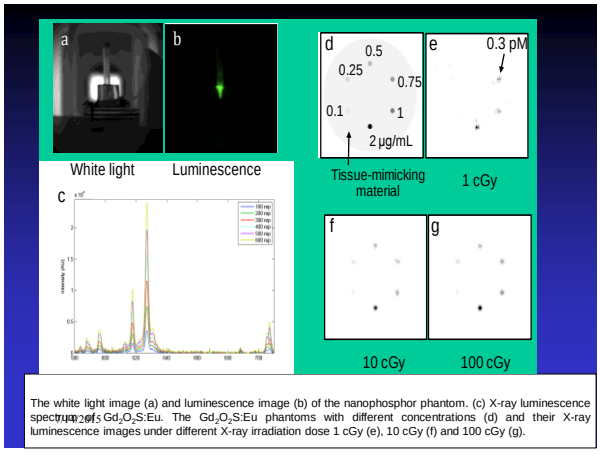

The white light image (a) and luminescence image (b) of the nanophosphor phantom. (c) X-ray luminescence spectrum of Gd_2O_2S:Eu. The Gd_2O_2S:Eu phantoms with different concentrations (d) and their X-ray luminescence images under different X-ray irradiation dose 1 cGy (e), 10 cGy (f) and 100 cGy (g).

SUMMARY

- Interaction of X-ay with endogenous or exogenous media provides the basis for highly sensitive X-ray molecular imaging.
- Highly sensitive XFCT is feasible.
- XFCT and XLCT are two examples of X-ray molecular/physiological imaging that are being developed at Stanford.